EFFECT OF CD SUBSTITUTION ON STRUCTURAL AND DIELECTRIC BEHAVIOR OF NIZN MIXED NANO FERRITES

D. S. Badwaik[1], S. P. Dongre, U. B. Mahatme, A. B. Sharma
[1]Kamla Nehru Mahavidyalaya, Nagpur. (India) 440009
[2]Bhalerao Science College, Saoner.(India)
[3]K. Z. S. Science College, Kalmeshwar.(India)
[4]Nabira College, Katol.(India)
Id-mail: badwaik_ds@rediffmail.com (corresponding Author)

Abstract:
A series of cadmium substituted mixed nickel zinc nano sized ferrites with composition $Ni_{0.5-X}Zn_{0.5}Cd_XFe_2O_4$ (X = 0, 0.1, 0.2, 0.3, 0.4, 0.5) were synthesized by sol gel auto combustion route. The structural and crystal phase of the nanocrystalline powders were characterized by X-ray powder diffraction pattern, which shows formation of single cubic spinel phase. The lattice parameter, X-ray density (Dx), experimental density (D), porosity (P), ionic radii, bond length and hoping length of the samples have been measured from XRD data. Results showed that the lattice parameter increased with increasing concentration of cadmium. The crystallite size is in the range 45- 62 nm, shows nano sized of prepared samples. The microstructure was studied by scanning electron microscopy (SEM) indicates the agglomerated spherical shape nanoparticles. The frequency dependent ac electrical conductivity, dielectric constant and loss tangent (tan δ) measured at room temperature, shows dielectric dispersion. Dielectric constant and loss tangent decreases with increase of frequency, indicating decrease in polarization. In fact, dielectric constant (ε') and loss tangent (tan δ) reaches a constant value for all the samples above certain higher frequency.
Keywords: Nano ferrites, auto combustion, structural analysis, AC electrical conductivity, Dielectric constant, SEM.

1. Introduction

Spinel ferrites are good dielectric materials because of their high resistivity and low loss behaviour and hence vast applications over a wide range of frequencies. The importance of the soft magnetic ferrites, in low frequency inductors, antenna rods and wide-band are well known and their uses in the fields have been continuously increasing for several decades. Nano crystalline ferrites are technologically important materials because of their unique electric, dielectric, magnetic and optical properties, which makes them useful for many applications like radio frequency circuits, microwave devices, transformer core, rod antennas, storage devices etc [1]. Hence it is important to study their dielectric behavior at different frequencies.

The study of DC electrical conductivity, ac electrical conductivity, dielectric constant, charge carriers concentration and charge carriers mobility give much information on the behaviour of the free and localized charge carriers. This leads to good explanation and understanding of the mechanism of electric conduction in the studied samples.

Nanoferrites are usually synthesized using various physical and chemical methods. The electrical conductivity and dielectric behavior in ferrites depends on many factors; preparation method, sintering temperature, amount and type of substitution. Several investigators have studied the frequency and temperature dependence of the dielectric constant [2, 3]. The nickel ferrites are the subject of extensive investigation because of their microwave applications such as circulators, isolators, phase shifters, etc., due to its low electrical conductivity, squareness of hysteresis loop [4,

5].The aim of the present work was to investigate the AC conductivity and dielectric constant of Cd substituted $Ni_{0.5-X}Zn_{0.5}Cd_XFe_2O_4$ (x = 0, 0.1, 0.2, 0.3, 0.4, 0.5) nano ferrites as a function of frequency at room temperature.. The study also includes effect of Cd^{2+} substitution on phase formation and conduction mechanism.

2. Experimental Details

A series of mixed nickel zinc nano ferrites substituted with Cd having chemical composition $Ni_{0.5-X}Zn_{0.5}Cd_XFe_2O_4$ (X = 0, 0.1, 0.2, 0.3, 0.4, 0.5) were synthesized by sol gel auto combustion method using Stoichometric proportion of 99.9% pure AR grade nickel nitrate ($Ni(NO_3)_2$,$6H_2O$), zinc nitrate ($Zn(NO_3)_2$, H_2O), cadmium nitrate ($Cd(NO_3)_2$,$4H_2O$) and ferric nitrate ($Fe(NO_3)_3$, $9H_2O$), as starting materials. Urea is used as fuel to supply requisite energy to initiate exothermic reaction amongst oxidants. Starting materials and fuel were dissolved in minimum amount of double distilled water; stirred the solution for 1h at room temperature to obtained uniform solution. Continue the stirring of the mixed nitrate aqueous solution on a magnetic hot-plate stirrer maintaining the temperature 60 °C. During the evaporation stages, solution became viscous and later on formed a viscous brown gel. Increase the temperature slowly above 60 °C, a sticky gel began to bubble for few minutes in a beaker. Finally gel got ignited automatically and burned with a glowing flint. The product of this reaction is fluffy loose powder of brown coloured ash could be termed as $Ni_{0.5-X}Zn_{0.5}Cd_XFe_2O_4$ presintered ferrite. The fluffy brown ash grinded in pestle mortal for 1h, then calcinated at 900 °C for 6 hours. Grind the samples again for 1h to get nano ferrites ready for characterization.

The X-ray diffraction pattern of the samples were obtained at room temperature by XPERT –PRO Diffractometer with Cu Kα radiation (λ=1.5406 °A). The surface morphology of the sample has been studied by scanning electron microscopy (ZEISS). The pallet of the samples for electrical conductivity measurement were made by using KBr dye punch of 10 mm diameter and applying pressure of 6 tons/cm^2 using hydraulic press (SES Roorky). Silver paste is applied on both sides of pallets for good electrical contacts. Electrical conductivity and dielectric parameters of the samples have been measured by two probe method using LCR-Q Bridge (HAMAG HM8118) meter.

3. Results and Discussion

3.1 Structural Analysis

The room temperature XRD patterns of all the samples of $Ni_{0.5-X}Zn_{0.5}Cd_XFe_2O_4$ ferrite system are shown in Fig. 1. The XRD pattern shows well defined Bragg's peaks. All the planes were indexed using Bragg's law, which confirmed the formation of cubic spinel structure in single phase. The strongest reflection comes from the (311) plane, which denotes the spinel phase. The peaks indexed to (220), (311), (222), (400), (422), (511) and (440) planes of a cubic unit cell, all planes are the allowed planes which indicates the formation of cubic spinel structure in single phase [6]. All observed peaks matched well with the characteristic reflections of nickel zinc ferrite (JCPDS Card No. 019- 0629). The samples were clean because no impurity characteristic peaks are observed in the XRD patterns. In addition, the patterns were also the same for all values of x, indicating that the crystal structure of the cadmium substituted samples remained the same as x = 0. The broadness of the peaks shows nano size of particles. The unit cell dimensions are determined from the d- spacing of a most intense peak (311) by making use of the cubic formula for inter-planer spacing.

$$a = d\,(h^2 + k^2 + l^2)^{1/2} \quad \text{Å}$$

Where “a” is the lattice constant, d- is interplaner spacing and (h, k, l) are the miller indices of the crystal planes

The experimental density (D) of the samples was calculated by using the relation

$$D = \frac{M}{V} \quad \frac{gm}{cm^3}$$

Where M is the mass of the pallet was determined using a digital balance (Mettler) and V is the volume of the pallet calculated by using its dimensions.

The theoretical density (X-ray density), D_x was calculated using the relation

$$Dx = \frac{Z\,M}{NV} \quad \frac{gm}{cm^3}$$

Where M is the molecular weight, N (6.023 * 10^{23} molecules / mole) is the Avogadro’s number, Z = 8 is the number of molecules for

spinel unit cell and V is the volume of unit cell. The porosity (P) is calculated using the relation

$$P = \frac{Dx-D}{Dx}$$

The X-ray diffraction data is further used to calculate the octahedral and tetrahedral ionic radii (r_B, r_A) sites, the bond length on octahedral (B-O) and tetrahedral (A-O) sites of cubic spinel structure by using Standely's equations [7].

$$r_B = \left(\frac{5}{8} - u\right)a - r(O^{2-})$$

$$r_A = \left(u - \frac{1}{4}\right)a\sqrt{3} - r(O^{2-})$$

Cation – anion distance at B- site (Octahedral bond length)

$$B - O = \left(\frac{5}{8} - u\right)a$$

Cation – anion distance at A- site (Tetrahedral bond length)

$$A - O = \left(u - \frac{1}{4}\right)a\sqrt{3}$$

Where "a" is lattice parameter; r (O^{2-}) is the radius of oxygen ion (1.35 Å); u is the oxygen ion parameter, for ideal spinel ferrite u= 3/8. Hoping length in octahedral sites (L_B) and in tetrahedral sites (L_A) which is nothing but the distance between the magnetic ions, have been calculated using the following equation,

$$L_B = a\left(\frac{\sqrt{2}}{4}\right)$$

$$L_A = a\left(\frac{\sqrt{3}}{4}\right)$$

The lattice parameter, X-ray density, experimental density, porosity and were calculated from the XRD data are itemized in Table 1. The lattice parameter demonstrated a linear increase with increasing cobalt content obeying Vegard's law. These variations in lattice parameter can be explained on the basis of lattice expansion. If the radius of substitute ion is larger than the replaced ion, the lattice expands and lattice parameter increases. In our prepared ferrites samples Cd^{2+} ions with radius 0.097 nm substitute Ni^{2+} ions with radius 0.069 nm, hence increase in lattice parameter is expected. Similar results were reported by other investigators [8]. Cell volume is found to increase from 591.64 to 626.56$Å^3$ with the increase of Cd^{2+} concentration. This increase in cell volume confirms the complete and successful replacement of smaller ionic radius Ni^{2+} ions by relatively larger ionic radius ion Cd^{2+}. The crystallite size has been calculated from most intense diffraction peak (311) using Debye Scherrer formula is also itemized in Table 1 is in range 45nm – 62nm.

It is observed that X-ray densities are higher in magnitude than the corresponding experimental densities. This may be due to the existence of pores which were developed during calcinations process. The x-ray density goes on increasing with Cd content with minute inconsistency. This increase in density can be explained on the basis of atomic weight. Since the atomic weight of Cd (112.40 amu) is higher than that of Ni (58.693 amu), the increase in x-ray density is expected. It is observed that experimental density increases with Cd content up to X = 0.2 and then decreases. The increase in experimental density up to X = 0.2 may be due to the formation of solid solution. It is assumed that all Cd^{2+} ions enter into the lattice during calcinations and activating of the lattice diffusion. This assumption of the formation of solid solution is confirmed by the increase in lattice parameter with Cd content [9]. The increase of the lattice parameter usually increases the diffusion path, leading to an increase of the rate of cation inter diffusion in the solid solution. After X = 0.2, density begins to decrease, this is attributed to the increased intra-granular porosity resulting from discontinuous grain growth as proposed by Coble and Burke [10]. The variation of porosity with Cd content shows opposite trend to that of experimental density.

The calculated values of mean ionic radius of the octahedral (B) "r_B", tetrahedral (A) "r_A" sites, the bond lengths on octahedral (B-O), tetrahedral (A-O) sites, hopping lengths in octahedral (L_B) and tetrahedral (L_A) sites are itemized in Table 2. It is seen that with increasing the content of Cd, the ionic radii (r_B, r_A) and bond length (B-O, A-O) increases which is due increase in lattice parameter. The mean tetrahedral ionic radius shows slow increase than that of the ionic radius of octahedral site with increasing the content of Cd. Similar results have been reported by other investigators [11]. The hopping lengths in the octahedral site (L_B) and tetrahedral site (L_A) which is nothing but the distance between the magnetic ions are also increases with increasing content of Cd. This shows that more energy is required for jumping of electrons between A and B-sites as a result of which the conductivity

decreases. Jump lengths are directly related with lattice constants. So increase of the lattice constant values consequently increases the jump lengths.

The intensities of the (220) and (440) planes are more sensitive to cations in tetrahedral and octahedral sites respectively [12, 13]. Ni^{2+} and Cd^{2+} ion prefers octahedral sites (B-sites) and tetrahedral sites (A- sites) respectively, whereas Fe^{3+} ions prefer both tetrahedral and octahedral sites. From **Table 1** it is observed that with increase in Cd^{2+} content, the intensity of (440) decreases. This is due to the decrease in Ni^{2+} ion in octahedral site with the increase in Cd^{2+} content which occupies tetrahedral sites. The increase in intensity of (220) plane may be due to the increase of Cd^{2+} content at tetrahedral site.

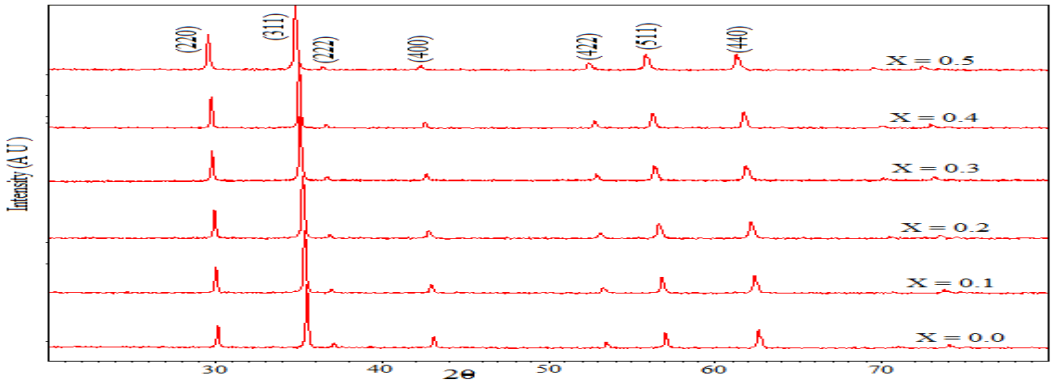

Figure 1 XRD spectra of $Ni_{0.5-X}Cd_X Zn_{0.5}Fe_2O_4$

Table1. Structural parameters of $Ni_{0.5-X}Zn_{0.5}Cd_XFe_2O_4$ calcinated at 900°C

Content of Cd	Lattice Parameter" a" Å	Unit cell vol.	X-ray density (Dx) gm/cm^3	Experimental density (D) gm/cm^3	Porosity % (P)	Particle size nm	Intensity of (220)	Intensity of (440)
X = 0.0	8.395	591.64	5.336	3.036	43	55	35.7	30.6
X = 0.1	8.425	598.01	5.399	4.010	25	45	41.8	28.3
X = 0.2	8.449	603.13	5.084	4.267	26	45	44.9	24.3
X = 0.3	8.486	611.09	5.510	4.158	24	45	45.1	23.3

Table 2. Ionic radii, bond length and hopping length on octahedral and tetrahedral sites of $Ni_{0.5-X}Zn_{0.5}Cd_XFe_2O_4$

Content of Cd	r_B Å	r_A Å	B-O Å	A-O Å	L_B Å	L_A Å
X = 0.0	0.748	0.465	2.098	1.815	2.967	3.630
X = 0.1	0.756	0.471	2.106	1.821	2.978	3.643
X = 0.2	0.762	0.477	2.112	1.827	2.986	3.654
X = 0.3	0.771	0.485	2.121	1.835	2.999	3.670
X = 0.4	0.775	0.488	2.125	1.838	3.004	3.676
X = 0.5	0.789	0.500	2.139	1.850	3.024	3.700

3.2 Scanning Electron Microscopy (SEM)

The surface morphology of Cd substituted $Ni_{0.5-X}Zn_{0.5}Cd_XFe_2O_4$ NPs were examined by analytical scanning electron microscope (SEM) shown in Fig. 2 for samples (X = 0.0 and 0.2) indicates the uniformly distributed agglomerated spherical shape nanoparticles of $Ni_{0.5-X}Zn_{0.5}Cd_XFe_2O_4$. This is attributed to the magnetic exchange interaction between the nanoparticles. The NPs with vivid pores suggesting it as more advantages for the gas sensing applications. Voids and pores present in prepared samples can be attributed to the release of gases during the combustion process and lesser the dense nature. It is also noticed

from SEM images that the grains are non uniformly distributed over the surface.

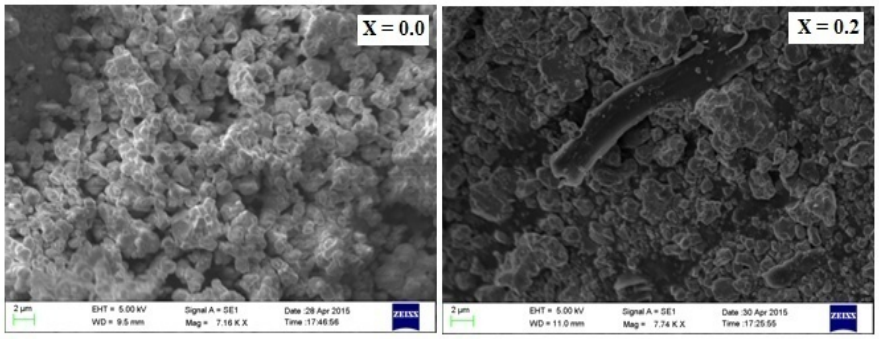

Fig. 2 SEM microograph of $Ni_{0.5-X}Zn_{0.5}Cd_XFe_2O_4$

3.3 Dielectric properties

To understand the conduction mechanism, the variation of AC conductivity with frequency at room temperature is depicted in Fig. 3. It is observed that AC conductivity increases with the frequency, which is the normal behavior of ferrites. The AC conductivity in ferrites is mainly due to exchange of electrons between the ions of same element but different valences. At lower frequencies increase in conductivity is less because non conductive grain boundaries are more active and hence the hopping of electron between $Fe^{2+} \leftrightarrow Fe^{3+}$ ions are less at lower frequencies. While at higher frequencies conductivity increases rapidly as the conductive grains become more active thereby promoting the hopping between $Fe^{2+} \leftrightarrow Fe^{3+}$ ions, thereby increasing the hopping conduction It is well known that AC conductivity in disordered solids is directly proportional to frequency [14]. Usually AC conductivity can be represented as,

$$\sigma_{AC} = \sigma_0(T) + \sigma(\omega,T)$$

This is the combination of frequency independent term $\sigma_0(T)$ called as DC conductivity and frequency dependent term $\sigma(\omega, T)$ called as AC conductivity due to hopping of electrons at octahedral site.

The frequency dependence variation of dielectric constant (ε') at room temperature is depicted in Fig.4. It is observed that, the dielectric constant shows an inverse dependence on frequency. The dielectric constant decreases rapidly with increasing frequency then it almost remains constant at higher frequencies. This dispersive behavior is similar to the conduction mechanism in the ferrite. The exchange of electrons between $Fe^{2+} \leftrightarrow Fe^{3+}$ gives the local displacement of electrons in the direction of applied electric field, which induces the polarization in ferrites and magnitude of exchange depends on the concentration of Fe^{2+}/Fe^{3+} ion pairs present at octahedral B site for the given ferrite [15]. Such types of behavior are reported earlier [16]. The dispersion occurring in the lower frequency regime is attributed due to Maxwell-Wagner type interfacial polarization and is in agreement with Koop's phenomenological theory [17]. However, at higher frequencies, the dielectric constant remains constant due to electronic polarization. In electronic polarization, electric dipoles are unable to follow the fast variation of applied alternating electric field resulting in low dielectric constant [18]. The frequency dependence variation of loss tangent at room temperature is depicted in Fig. 5. This shows the similar kind of dispersion relation. At lower frequency the value of tanδ is high and it decreases rapidly in low frequency regime then remains constant at higher frequencies. The high value of loss tangent corresponds to high resistivity grain boundaries within the material. Therefore, more energy is required for electron exchange between Fe^{3+} and Fe^{2+} ions resulting into high energy loss. At the higher frequency small amount of energy is required for electron exchange between Fe^{3+} and Fe^{2+} ions resulting into small value of energy loss and hence low value of electrical resistivity [19]. This gives the idea about the conduction mechanism within the ferrites. Among all samples x = 0.2 Cd substituted NiZn ferrite shows the highest loss

tangent value of 2.6 at low frequency. The low values loss tangent makes all samples potential candidate for microwave applications.

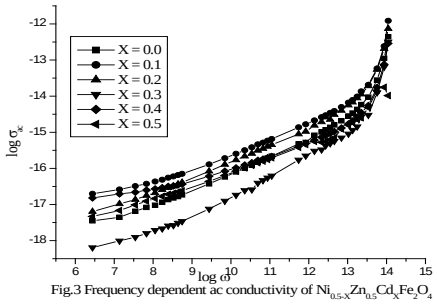

Fig.3 Frequency dependent ac conductivity of $Ni_{0.5-X}Zn_{0.5}Cd_XFe_2O_4$

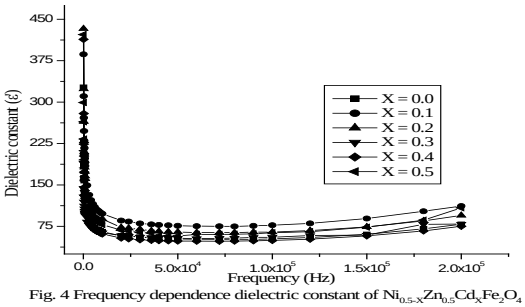

Fig. 4 Frequency dependence dielectric constant of $Ni_{0.5-X}Zn_{0.5}Cd_XFe_2O_4$

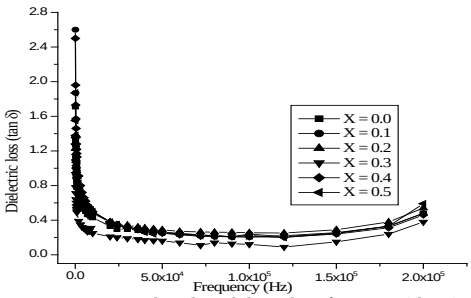

Fig. 5 Frequency dependence dielectric loss of $Ni_{0.5-X}Zn_{0.5}Cd_XFe_2O_4$

4. Conclusions

The cd substituted nickel zinc nano ferrites with chemical composition $Ni_{0.5-X}Zn_{0.5}Cd_XFe_2O_4$ have been successfully prepared by microwave assisted sol gel auto combustion rout. The X-ray diffraction patterns confirmed the formation of single phase cubic spinel structure. The average crystallite size of particles obtained from X-ray data is found in the range 45 nm to 62 nm. The lattice parameter "a" increases with content of Cd is due to the smaller radius ion replaced by larger one. The x-ray density also increases with Cd content, is attributed to the higher atomic weight of Cd comparing to Ni. SEM micrograph shows uniformly distributed spherical shape agglomerated nanoparticles. The AC conductivity increases with increase in frequency, whereas dielectric constant and loss tangent decreases with frequency.

References

1. S. Gubbala, H. Nathani, K. Koziol and R. D. K. Misra, (2004) "Magnetic Properties of Nanocrystalline Ni-Zn, Zn-Mn, and Ni-Mn Ferrites Synthesized by Reverse Micelle Technique," Physica B: Condensed Matter, Vol. 348, No. 1-4, pp. 317-328.
2. A.M. Abo ElAta,M.A.ElHiti, J. Phys. III (France) 7 (1997) 883.
3. M.A. El Hiti, M.A. Ahmed, M.M. Mosaad, S.M. Attia, J. Magn. Magn. Mater. 150 (1995) 399.
4. A.S. Waingankar, S.G. Kulkarni, M.S. Sagare, J. Phys. IV (1997) 155.
5. O.H. Kwon, Y. Fukushima, M. Sugimoto, N. Hiratsuka, J. Phys. IV (1997) 165.
6. S.A. Mazen, S.F. Mansour, H.M. Zaki, published on line 15 June 2003. "Some physical and magnetic properties of Mg-Zn ferrite". Cryst. Res. Technol. 38, No 6,471-478 (2003).
7. J. Standely, Oxide Magnetic Materials, Ciarendon, Oxfird, UK, 1972.
8. S. S. Bellad, andB. K. Chougule, (2000, Sept) "Composition and frequency dependent dielectric properties of Li-

Mg-Ti ferrites." J Mater. Chem. Phys. 66(1), 58-63.
9. Sajal Chandra Mazumdar, A. K. M. Akther Hossain " Synthesis and Magnetic Properties of $Ba_2Ni_{2-X}Zn_XFe_{12}O_{22}$ Hexaferrites" World Jour. Of Condensed Matter Physics, 2012, 2, 181-187.
10. Z. Yang, C. S. Wang, X. H. Li, H. X. Zeng, Mater Sci. Eng. :B 90, (1-2) (2002) 142-145.
11. N. M. Deras and A. Alarifi, J. Anal. Appl. Pyrolysis, 2011.
12. B. P. Ladgaonkar and A. S. Vaingainkar, "X-ray Diffrac tion Investigation of Cation Distribution in CdxCu(1-x) Fe2O4," Materials Chemistry and Physics, Vol. 56, No. 3, 1998, 280-283
13. C. S. Narasimhan and C. S. Swamy, "Studies on the Solid State Properties of the Solid Solution Systems. $MgAl_{(2-x)}Fe_xO_4$," Physica Status Dolidi (a), Vol. 59, 1980 p. 817.
14. R.C. Kambale, P. Shaikh, C.H. Bhosale, K.Y. Rajpure, and Y.D. Kolekar, Smart Mater. Struct. 18, 085014 (2009).
15. K.A. Hossain, S. Akther, and D.K. Saha, 37, 73 (2013).
16. N.D. Patil, N.B. Velhal, N.L. Tarwar, and V.R. Puri, 3, 73 (2014).
17. C. G. Koops, "On the Dispersion of Resistivity and Dielectric Constant of Some Semiconductors at Audio frequencies", Physics review. Vol. 83, pp. 121, (1951).
18. K. B, N.S.N. K. Permar, and A. Sharma, Res. J. Mater. Sci. 1, 7 (2013).
19. R. C. Kambale, P. A. Shaikh, C. H. Bhosale, K. Y. Rajpure, Y. D. Kolekar, "The effect of Mn substitution on the magnetic and dielectric properties of cobalt ferrite synthesized by an auto combustion route", Smart Material Structure, Vol. 18, pp. 115028, (2009).